Spectrochimica Acta Part A: Molecular and Biomolecular Spectroscopy 117 (2014) 42–53

Contents lists available at ScienceDirect

Spectrochimica Acta Part A: Molecular and Biomolecular Spectroscopy

journal homepage: www.elsevier.com/locate/saa

Quantum mechanical and spectroscopic (FT-IR, ^{13}C, ^{1}H NMR and UV) investigations of potent antiepileptic drug 1-(4-chloro-phenyl)-3-phenyl-succinimide

Vesna D. Vitnik [a,*], Željko J. Vitnik [a], Nebojša R. Banjac [b], Nataša V. Valentić [b], Gordana S. Uščumlić [b], Ivan O. Juranić [a]

[a] Department of Chemistry, IChTM, University of Belgrade, Studentski trg 12-16, 11001 Belgrade, Serbia
[b] Department of Organic Chemistry, Faculty of Technology and Metallurgy, University of Belgrade, Karnegijeva 4, 11120 Belgrade, Serbia

HIGHLIGHTS

- Experimental and theoretical vibrational and NMR spectra are investigated.
- The PED calculation regarding the normal modes provides a strong support for the frequency assignment.
- The absorption spectrum has been calculated in solvent environment using CPCM model.
- HOMO–LUMO, NBO and chemical reactivity analysis were also performed.
- Molecular electrostatic potential of the title compound was calculated.

GRAPHICAL ABSTRACT

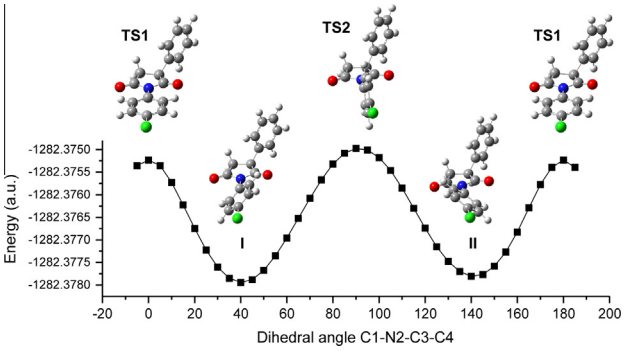

ARTICLE INFO

Article history:
Received 16 March 2013
Received in revised form 20 July 2013
Accepted 31 July 2013
Available online 7 August 2013

Keywords:
1-(4-Chloro-phenyl)-3-phenyl-succinimide
Vibrational spectra
NMR
UV–Vis
NBO
TD-DFT

ABSTRACT

This study represents an integrated approach towards understanding the vibrational, electronic, NMR, and structural aspects, and reactivity of 1-(4-chloro-phenyl)-3-phenyl-succinimide (CPPS). A detailed interpretation of the FT-IR, UV and NMR spectra were reported. The equilibrium geometry, bonding features, and harmonic vibrational frequencies have been investigated with the help of density functional theory (DFT) B3LYP method using 6-31G(d,p) and 6-311++G(d,p) basis set. The scaled theoretical wavenumber showed very good agreement with the experimental values. The ^{1}H and ^{13}C nuclear magnetic resonance (NMR) chemical shifts of the molecule were calculated by the Gauge-Invariant Atomic Orbital (GIAO) method. Stability of the molecule, arising from hyperconjugative interactions and charge delocalization, has been analyzed using Natural Bond Orbital (NBO) analysis. The results show that ED in the σ^* and π^* antibonding orbitals and second order delocalization energies $E(2)$ confirm the occurrence of intramolecular charge transfer (ICT) within the molecule. UV–Vis spectrum of the compound was recorded and the electronic properties, such as HOMO and LUMO energies, were calculated by Time-Dependent DFT (TD-DFT) approach. To estimate chemical reactivity of the molecule, the molecular electrostatic potential (MEP) surface map is calculated for the optimized geometry of the molecule.

Introduction

Imides and their derivatives have been considered as an important class of nitrogen-containing heterocycles. There has been increasing interest in the study of succinimides due to their

* Corresponding author. Tel.: +381 113336735; fax: +381 112636061.
E-mail address: vesnak@chem.bg.ac.rs (V.D. Vitnik).

1386-1425/$ - see front matter © 2013 Elsevier B.V. All rights reserved.
http://dx.doi.org/10.1016/j.saa.2013.07.099

anticonvulsant activity. Ethosuximide [1] is a succinimide anticonvulsant, used mainly in absence seizures. Ethosuximide has also been shown to have neuroprotective [2], antinociceptive and lifespan-extending effects [3] and has the potential for treating several neuropsychiatric disorders, including Parkinson's disease, methamphetamine-induced stereotyped behavior and alcohol dependence [4–6]. Methsuximide is an anticonvulsant with the therapeutic efficacy due to its pharmacologically active metabolite, *N*-desmethylmethsuximid [7]. Phensuximide used to treat epilepsy and other seizure disorders [8].

Substituted succinimide rings are also found in some pharmacologically active natural products, such as Rebeccamycin [9] (which shows significant antitumor properties *in vitro* [10]) and Methyllycaconitine [11] (which has been explored as a possible therapeutic agent for the treatment of spastic paralyses in man [12] and has been shown to have insecticidal properties, too [13]).

Numerous compounds possessing a succinimide ring exhibit pharmacological activity such as antitumor [14], sedative and tranquilizer [15], hypnotic [16], hypotensive [17], diuretic [18], tuberculostatic-antitubercular [19] and antidepressant [20].

Succinimides and their derivatives are known for their broad spectrum of biological activity as: plant growth regulator [21], antifungal [22], antimicrobial [23,24] and insecticidal activity [25].

In addition, succinimide have applications in various other fields, for example, they are employed as polymers, activators and stabilizers, vulcanizing agents, lubricant additives, dyes and optical brightening agents, photographic and printing aids [26].

The most typical feature of succinimide derivatives is that the pharmacological and spectroscopic properties can be readily modified by introduction of substituents in the succinimide ring. Thus, two series of succinimide derivatives were synthesized and their properties relevant to pharmacokinetics have been studied [27]. Compound 1-(4-chloro-phenyl)-3-phenyl-succinimide (abbreviated as CPPS) is one of the four agents picked as the best promising candidates regarding human intestinal absorption and plasma protein binding properties.

Although new developments in syntheses have been reported, structural and spectroscopic properties of such compounds was not extensively studied [28,29]. Detailed knowledge on the structure and spectra of succinimides is a necessary prerequisite for understanding their chemical and biological properties. In our ongoing investigation on the synthesis of succinimide derivatives, we herein describe our results on CPPS (previously synthesized by us [27]) concerning the structural, vibrational, electronic, NMR and reactivity analyses through spectral measurements. The vibrational spectra of CPPS molecule have been thoroughly analyzed to identify the various normal modes with greater wavenumber accuracy. Density Functional Theory B3LYP/6-311++G(d,p) calculations have been performed to support our wavenumber assignments. The redistribution of Electron Density (ED) in various bonding, antibonding orbitals and $E(2)$ energies have been calculated by Natural Bond Orbital (NBO) analysis to provide evidence of stabilization originating from the hyperconjugation and various intramolecular interactions. The UV spectroscopic studies along with HOMO, LUMO analysis have been used to elucidate information regarding charge transfer within the molecule. Moreover, molecular electrostatic potential (MEP) surface is plotted over the optimized geometry to explicate the reactivity of CPPS molecule. To our best knowledge, this is the first report on the computational study of CPPS. The calculated results were compared with the experimental and the observed spectra were analyzed in detail. Calculated vibration wavenumbers, UV–Vis absorption wavelengths and NMR chemical shift values are in good agreement with the experimental results.

Experimental details

The chemical structure and purity of the synthesized compound [27] was confirmed by its melting point, ^{1}H and ^{13}C NMR, FT-IR and UV spectra. FT-IR spectrum in the region 4000–400 cm^{-1} using a KBr pellet technique at a resolution of 1 cm^{-1}, was recorded with a Bomem MB 100 spectrophotometer. The ultraviolet absorption spectrum of CPPS was examined in the range 200–500 nm using Shimadzu 1700 UV–Vis spectrophotometer. The UV pattern was taken from a 10^{-5} molar solution of CPPS, dissolved in ethanol. ^{1}H and ^{13}C NMR spectra were recorded in $CDCl_3$ and DMSO-d_6 using TMS as an internal standard on a Bruker Avance 500 spectrometer at 500 MHz and 125 MHz, respectively.

Computational details

We did our best to meet the requirements of both accuracy and computing economy, theoretical methods and basis sets should be considered. DFT has proved to be extremely useful in treating electronic structure of molecules. Initial geometry generated from standard geometrical parameters was minimized without any constraint in the potential energy surface at B3LYP level, adopting the standard 6-31G(d,p) basis set. The geometries of the most stable conformers **I** and **II** of CPPS were then reoptimized at B3LYP/6-311++G(d,p) level for better description. All the calculations were done using Gaussian 03 program package [30]. Optimized structural parameters were used in the vibration frequency, the electronic properties, and the isotropic chemical shift calculations. The validity of the optimized geometry was confirmed by frequency calculations, which gave real values for all the obtained frequencies.

The assignment of the calculated wavenumbers was aided by the animation option of Gauss View 3.0 graphical interface from Gaussian programs. Furthermore, the theoretical vibrational spectra of the title compound are interpreted by means of Potential Energy Distribution (PED) using VEDA 4 program [31]. The harmonic frequencies were calculated by B3LYP method using 6-311++G(d,p) basis set. However, the vibrational frequency values computed at this level contain known systematic errors [32,33]. Therefore, it is customary to scale down the calculated harmonic frequencies in order to improve the agreement with the experiment. The theoretical spectrum of CPPS was scaled with 0.958 (for wavenumbers over 1700 cm^{-1}) and 0.983 (for wavenumbers under 1700 cm^{-1}) [34].

The nuclear magnetic resonance (NMR) chemical shifts calculations were performed using Gauge-Invariant Atomic Orbital (GIAO) method [35,36] at B3LYP level with 6-311++G(d,p) basis set. The ^{1}H and ^{13}C isotropic chemical shifts were referenced to the corresponding values for TMS, which was calculated at the same level of theory. The effect of solvent on the theoretical NMR parameters, as well as on the stability of CPPS molecule, was included using Conductor Polarizable Continuum Model (CPCM) provided by Gaussian 03 [30]. Dimethyl sulfoxide (DMSO) and chloroform ($CHCl_3$) were used as solvents.

In order to evaluate the energetic and dipole moment behavior of conformers **I** and **II** of CPPS in solvent media, we also carried out optimization calculations in six solvents ($\varepsilon = 4.711$, $CHCl_3$; $\varepsilon = 10.125$, CH_2ClCH_2Cl; $\varepsilon = 24.852$, C_2H_5OH; $\varepsilon = 37.219$, DMF; $\varepsilon = 46.826$, DMSO; $\varepsilon = 78.355$, H_2O) at the B3LYP/6-31G(d,p) level using the CPCM method [37].

UV absorption energies of this compound were calculated by TD-DFT method in ethanol solvent. The frontier molecular orbital energies, energy gap between various occupied and unoccupied molecular orbitals of CPPS are also calculated at the same level of DFT theory.

The NBO analysis [38] was performed using NBO 3.1 program as implemented in the Gaussian 03 package [30] at the B3LYP/6-311++G(d,p) level in order to understand various second order interactions between the filled orbitals of one subsystem and vacant orbitals of another subsystem, which is a measure of the intramolecular delocalization or hyperconjugation.

To reveal chemical reactivity of the molecule, the MEP surface, for the 0.002 a.u. isosurfaces of electron density, is plotted over the optimized geometry of stable isomer **I** of CPPS.

Results and discussions

Conformational stability

The aim of the conformational analysis of the CPPS molecule is to provide a model for the molecular structure. For this reason, the energy barriers of rotation around the N2—C3 bond were calculated at the B3LYP with 6-31G(d,p) basis set. The potential energy surface (PES) scan for our title molecule is shown in Fig. 1. During the calculation, all the geometrical parameters were simultaneously relaxed while the dihedral angle C1—N2—C3—C4 (around N2—C3 bond, see Fig. 2 for atom numbering scheme) was varied form 0° to 180° by steps of 5°. For this rotation two-minima energy curve has been obtained (at 40° and 140°) as shown in Fig. 1 clearly demonstrates that 40° corresponds to conformer **I** (−1282.3779 a.u.), and 140° corresponds to conformer **II** (−1282.3778 a.u.). The geometries of the most stable conformers **I** and **II** of CPPS, reoptimized at B3LYP level using 6-311++G(d,p) basis set, are shown in Fig. 2.

The molecular geometries are constrained through two effects acting oppositely: a repulsion of the carbonyl groups of succinimide (ring 1) and hydrogen atoms H18 and H24 in *ortho* positions on the chloro-substitued phenyl group (ring 2), which would lead to a staggered conformation of the molecule, and a conjugation effect, which tends to bring 4-chloro-phenyl group in the succinimide plane. The equilibrium geometry of the molecule results from a balance between these two effects. The two minima occurring at variation of the torsional angles are not identical because the phenyl group (ring 3) in position 3 of succinimide ring.

A maximum (**TS2**) is found for a dihedral angle of 90° (E_{90}, perpendicular conformation) with a barrier height of about at 1.866 kcal/mol (B3LYP/6-31G(d,p). Nevertheless, other maximum (**TS1**) is found for a dihedral angle of 0° (E_0, coplanar conformation). The calculated results show that E_0 has energy ≈0.165 kcal/mol lower than the E_{90}.

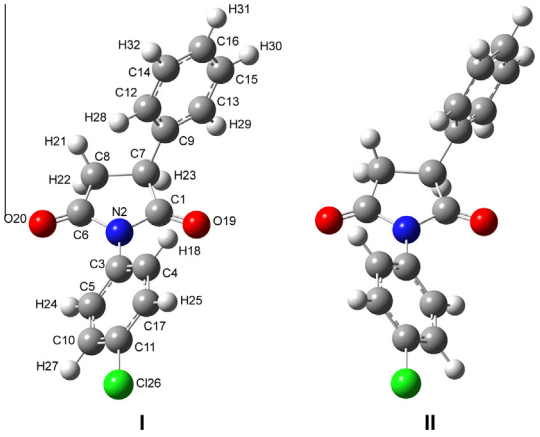

Fig. 2. Stable conformers **I** and **II** of CPPS.

Molecular geometry

The optimized geometrical parameters of conformer **I** of CPPS calculated by B3LYP level with 6-311++G(d,p) basis set are listed in Table 1, which are in accordance with the atom numbering scheme given in Fig. 2 for CPPS. There is no exact X-ray crystal structure for CPPS and hence we cannot compare our theoretical results with experimental data.

Vibrational analysis

The title molecule CPPS has 32 atoms, belongs to C1 point group and possesses 90 normal vibration modes. The calculated frequencies are slightly higher than the observed values for the majority of the normal modes. Two factors may be the reason for the discrepancies between the experimental and computed spectra of this compound. The first is the influence of the environment and the second one is the fact that the experimental value is an anharmonic frequency while the calculated value is a harmonic frequency. The calculated harmonic wavenumber are usually higher than the corresponding experimental quantities because of the combination of electron correlation effects and basis set deficiencies. Uniform scaling procedure is adopted in this

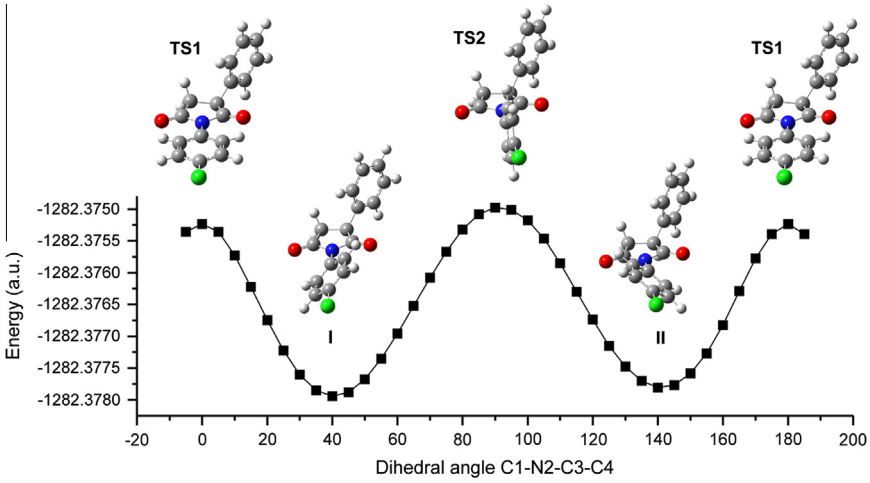

Fig. 1. The potential energy curve of CPPS along the C1—N2—C3—C4 dihedral angle, calculated by B3LYP/6-31G(d,p) level of theory.

Table 1
Selected molecular structure parameters of conformer I of CPPS.

Bond lengths (Å)		Bond angles (°)			
R(1,2)	1.408	A(2,1,7)	108.4	A(5,10,27)	120.4
R(1,7)	1.538	A(2,1,19)	125.1	A(11,10,27)	120.2
R(1,19)	1.203	A(7,1,19)	126.5	A(10,11,17)	121.1
R(2,3)	1.431	A(1,2,3)	123.4	A(10,11,26)	119.5
R(2,6)	1.408	A(1,2,6)	112.8	A(17,11,26)	119.4
R(3,4)	1.395	A(3,2,6)	123.8	A(9,12,14)	120.7
R(3,5)	1.395	A(2,3,4)	119.8	A(9,12,28)	120.3
R(4,17)	1.391	A(2,3,5)	120.1	A(14,12,28)	119.0
R(4,18)	1.082	A(4,3,5)	120.2	A(9,13,15)	120.7
R(5,10)	1.391	A(3,4,17)	120.0	A(9,13,29)	119.6
R(5,24)	1.081	A(3,4,18)	120.2	A(15,13,29)	119.7
R(6,8)	1.518	A(17,4,18)	119.8	A(12,14,16)	120.2
R(6,20)	1.205	A(3,5,10)	120.0	A(12,14,32)	119.7
R(7,8)	1.539	A(3,5,24)	120.2	A(16,14,32)	120.1
R(7,9)	1.520	A(10,5,24)	119.8	A(13,15,16)	120.1
R(7,23)	1.092	A(2,6,8)	108.0	A(13,15,30)	119.7
R(8,21)	1.091	A(2,6,20)	125.1	A(16,15,30)	120.1
R(8,22)	1.093	A(8,6,20)	126.9	A(14,16,15)	119.6
R(9,12)	1.400	A(1,7,8)	104.2	A(14,16,31)	120.2
R(9,13)	1.397	A(1,7,9)	110.9	A(15,16,31)	120.2
R(10,11)	1.391	A(1,7,23)	105.9	A(4,17,11)	119.3
R(10,27)	1.082	A(8,7,9)	115.9	A(4,17,25)	120.4
R(11,17)	1.391	A(8,7,23)	111.2	A(11,17,25)	120.2
R(11,26)	1.757	A(9,7,23)	108.2	Dihedral angles (°)	
R(12,14)	1.393	A(6,8,7)	106.3	D(7,1,2,3)	−177.8
R(12,28)	1.085	A(6,8,21)	109.0	D(7,1,2,6)	3.0
R(13,15)	1.394	A(6,8,22)	108.1	D(19,1,2,3)	2.2
R(13,29)	1.085	A(7,8,21)	113.7	D(19,1,2,6)	−176.9
R(14,16)	1.394	A(7,8,22)	112.6	D(2,1,7,8)	−5.2
R(14,32)	1.084	A(21,8,22)	107.0	D(2,1,7,9)	120.3
R(15,16)	1.393	A(7,9,12)	121.2	D(19,1,7,8)	174.8
R(15,30)	1.084	A(7,9,13)	120.1	D(19,1,7,9)	−59.8
R(16,31)	1.084	A(12,9,13)	118.7	D(1,2,3,4)	47.3
R(17,25)	1.082	A(5,10,11)	119.4	D(1,2,3,5)	−132.7

work to eliminate errors in the harmonic wavenumber output. Based on this procedure, the theoretical harmonic wavenumbers have been scaled by the factor of 0.958 and 0.983 in the region from 3200 to 1700 cm^{-1} and lower than 1700 cm^{-1}, respectively [34]. The standard scaling factors could be used to model the entire vibrational spectrum of the present compound since it is "well behaved", in that the molecules weakly interact with each other in the solid phase (they are not connected via, say, hydrogen bonds). For comparison, scaled theoretical and experimental FT-IR wavenumbers are summarized in Table 2 along with detailed vibrational assignments and calculated IR intensities, the theoretically computed wavenumbers matched well with the experimental ones. Similarly, the comparison of the experimental and calculated FT-IR spectra are also presented in Fig. 3. The detailed assignments along with the percentage of PED are summarized in Table 2, where the assignments having <10% (PED percentage) are ignored.

After scaling, we drawn correlation graph between the experimental (FT-IR) and calculated wavenumbers (Fig. S1) (Supplementary material). The relation between these results is linear and described by the following equation:

$$\nu_{cal.} = 1.0065\nu_{exp.} - 2.6536 \quad (R^2 = 0.9985, \mathrm{RMSD} = 27.86\ cm^{-1})$$

Comparison of the scaled wavenumbers calculated by the B3LYP method using 6-311++G(d,p) basis set with experimental values, reveals that this method exerts a very good agreement having correlation coefficients of 0.9985 and the root-mean-square deviations 27.86 cm^{-1}.

Ring vibrations

The C—H stretching vibrations of aromatic and heteroaromatic structures generally occur in the region 2800–3100 cm^{-1} [39]. This permits the ready identification of the structure. The bands in this region are not much affected by the nature and position of the substituents. The theoretical description for this region is somewhat difficult due to the low intensity of C—H stretching modes. For CPPS, the C—H stretching ring vibrations are predicted at 3024–3083 cm^{-1} for B3LYP/6-31++G(d,p) level of theory. These vibrations observed experimentally at 3030, 3070 and 3095 cm^{-1} in the FT-IR spectrum for CPPS. The scaled theoretical values of ring C—H stretching modes coincide well with that of experimental data as depicted in Table 2. The percentage of PED predicts that C—H modes of CPPS are very pure, since their percentage is almost 100%. However, C—H stretching modes also satisfy harmonic oscillator equation [40]. The C—H stretching modes of CPPS are predicted to be in the range 2937–3083 cm^{-1} by B3LYP/6-311++G(d,p). A comparison with the results from the normal mode analysis of CPPS shows that the aromatic C—H stretching vibrations around 3070 cm^{-1} remain unaltered by chlorine substitution.

The benzene ring C—H in-plane bending vibrations are usually weak and observed in the region 1000–1300 cm^{-1}, while the C—H out-of-plane bending vibrations lie in the region 650–900 cm^{-1} [39]. In-plane C—H bending vibrations are observed in the range of 1035–1558 cm^{-1} for CPPS in the FT-IR spectrum. The in-plane bending vibrations of 4-chloro-phenyl part, ring 2, in CPPS are observed as intense bands at 1299 and 1493 cm^{-1} in IR and the corresponding calculated value are 1310 and 1498 cm^{-1}. In-plane C—H bending vibrations of CPPS molecule observed at 1075 and 1198 cm^{-1} in the FT-IR spectrum which are mixed with stretching C—C vibrations. The out-of-plane C—H

Table 2
Vibrational wavenumbers obtained for CPPS at B3LYP/6-311++G(d,p) method [harmonic frequency (cm^{-1}), IR_{int} (K $mmol^{-1}$)].

Normal mode no.	Experimental wavenumbers (cm^{-1})	Theoretical wavenumbers (cm^{-1})			Assignments, PED(%)[b]
		B3LYP unscaled	B3LYP scaled	IR_{Int}[a]	
1	3095	3218	3083	0.42	ν_{sym}CH, ring 3, (96)
2		3216	3081	0.61	ν_{sym}CH, ring 3, (96)
3		3201	3066	0.79	ν_{asy}CH, ring 3, (98)
4		3199	3065	1.99	ν_{asy}CH, ring 3, (97)
5	3070	3192	3058	13.21	ν_{sym}CH, ring 2, (93)
6	3030	3181	3048	22.21	ν_{sym}CH, ring 2, (93)
7		3173	3039	6.31	ν_{sym}CH, ring 2, (98)
8		3164	3031	1.55	ν_{asy}CH, ring 2, (93)
9		3157	3024	7.95	ν_{asy}CH, ring 2, (94)
10	2923	3114	2983	2.05	$\nu_{asy}CH_2$, (99)
11		3075	2946	5.26	$\nu_{sym}CH_2$, (99)
12	2853	3066	2937	6.12	$\nu_{sym}CH_2$, (100)
13	1780	1839	1762	17.76	νCO (88)
14	1708	1777	1702	637.2	νCO (89)
15	1629	1643	1615	6.35	νCC, ring 3, (39)
16	1601	1634	1606	1.77	νCC, ring 2, (40)
17	1595	1625	1597	0.87	νCC, ring 3, (48) + βCCC(10)
18	1589	1619	1591	0.73	νCC, ring 2, (57)
19	1558	1527	1501	7.99	βCCH, ring 3, (66)
20	1493	1524	1498	171.18	βCCH (63), ring 2
21		1486	1461	8.01	βCCH, ring 3, (44)
22	1455	1468	1443	5.94	δCH_2 (84)
23	1420	1438	1413	2.66	νCC (39) + βCCH, ring 3, (22)
24	1401	1376	1353	382.78	νCN (53)
25	1341	1372	1349	15.92	βCCH, ring 3 (76)
26		1347	1324	0.86	νCC (44) + βCCH, ring 3, (24)
27	1299	1333	1310	2.81	νCC (15) + βCCH, ring 2, (68)
28		1319	1297	3.19	νCC, ring 2, (77)
29	1279	1306	1283	3.44	νCC (12) + τCCCH (15) + τCCCN (47)
30		1300	1278	0.36	νCC (11) + τ CCCH (15)
31	1234	1257	1236	2.75	ωCH_2 (14) + τCCCH (34)
32		1215	1194	5.77	νCC (40) + βCCH (33)
33		1208	1187	0.54	βCCH, ring 3, (75)
34		1205	1185	2.27	νCC (11) + βCCH, ring 2, (67)
35	1198	1186	1166	59.76	νCN (13) + νCC (12) + βCCH, ring 2, (10)
36	1165	1185	1165	1.45	βCCH, ring 3, (70)
37	1100	1180	1160	8.34	tCH_2 (36) + τNCCH (16)
38	1092	1175	1155	227.35	νCN (17) + νCC (17)
39	1075	1134	1115	9.47	νCC (28) + βCCH, ring 2, (58)
40	1035	1108	1089	5.94	νCC (33) + βCCH, ring 3, (45)
41	1017	1102	1083	78.71	νCN (50) + νCCl (19)
42		1059	1041	2.4	νCC (12) + βCCN, ring 1, (21)
43		1053	1035	4.57	νCC, ring 3, (29)
44		1036	1018	1.73	νCC, ring 3, (17) + βOCN, ring 1, (10)
45	1000	1033	1015	25.73	βCCC, ring 2, (79)
46	971	1017	1000	2.33	νCC (21) + βCCC, ring 3, (60)
47		1004	987	0.02	τCCCH, ring 3, (68) + τCCCC, ring 3, (12)
48		984	967	0.11	τCCCH, ring 3 (91)
49		973	956	1.65	τCCCH, ring 2 (65)
50	950	972	955	4.53	ρCH_2 (11) + γCNCO, ring 1, (12)
51	928	954	938	3.52	τCCCH, ring 2, (80)
52	894	935	919	17.35	τCCCH, ring 3 (33)
53		921	906	8.84	νCC, ring 1, (11) + τCCCH, ring 3, (41)
54		853	839	0.02	τCCCH, ring 3, (100)
55	842	841	827	32.07	τCCCH, ring 2, (52) + γCCCN (11)
56	826	823	809	0.21	τCCCH, ring 2, (100)
57	818	818	804	10.5	τCCCC (10) + γCNCO, (17)
58	791	799	785	24.13	νCC (14) + βCCC (21)
59	757	756	744	40.95	τCCCH, ring 3, (22) + τCCCC (20)
60	733	736	724	9.22	νCCl (10) + βCCC, ring 2, (11)
61		717	705	4.61	τCCCC, ring 2, (67)
62	702	711	698	41.24	τCCCC, ring 2, (50) + τCCCH, ring 3, (37)
63	654	668	657	35.78	γCCN, ring 1 (30) + βCCC, ring 3 (12)
64	650	648	637	2.99	βCCC, ring 1, ring 2, (37)
65	616	639	628	6.52	νCN (16) + βCNC (24)
66	610	631	620	5.1	βCCC, ring 3, (63)
67		627	617	2.55	βCCO (17)
68	565	578	569	1.89	τNCCH (17) + γCNCO (35)
69		540	531	0.59	βCCC, ring 3, (15) + γCNCO (12)
70	531	533	524	9.39	νCCl (15)
71	510	512	503	16.52	γCCCCl (13) + γNCCC (14)
72	488	496	488	10.79	τCCCC, ring 3, (21)
73	424	427	419	32.93	νCCl (21) + βCCO (19)

Table 2 (*continued*)

Normal mode no.	Experimental wavenumbers (cm^{-1})	Theoretical wavenumbers (cm^{-1})			Assignments, PED(%)[b]
		B3LYP unscaled	B3LYP scaled	IR_{Int}[a]	
74		420	413	0.35	τCCCH (24) + τCCCC, ring 2 (68)
75	418	414	407	0.33	τCCCH (10) + τCCCC, ring 3, (51)
76	402	412	405	4.49	βCCC (11) + βCCN (24)
77		349	344	0.36	βCNC (10) + τCCCC, ring 2, (25) + γCCCCl (27)
78		313	308	1.2	νCC (13) + βCCC (14) + βCCN (15)
79		282	277	1.88	βCCCl (41)
80		262	257	1.44	βCCCl (17)
81		225	221	0.77	βCCC (38)
82		204	200	1.35	τCCCC (13)
83		172	169	1.35	βCNC (27) + τCCCC, ring 2, (12) + γCCCCl (29)
84		129	126	5.31	βCNC (11) + βCNC (16) + τCCNC (20) + γCCCN (22)
85		105	103	3.15	βCCC (25) + τCCCC (37)
86		58	57	0.2	βCNC (12) + τCCCC (33) + γCCCN (26)
87		53	52	0.89	τCNCC (45) + τCCCN (12)
88		39	38	0.4	βCCC (10) + τCCCC (10) + τCNCC (45) + τCCCN (13)
89		28	28	0.08	τCCCC (72)
90		11	11	0.02	βCCC (13) + τCCCN (48) + τCCNC (18)

[a] IR_{Int} – IR intensity; K $mmol^{-1}$.
[b] PED less than 10% are not shown; ν – stretching; ν_{sym} symmetric stretching; ν_{asy} – asymmetric stretching; β – in plane bending; γ – out-of-plane bending; ω – wagging; t – twisting; δ – scissoring; τ – torsion, ρ – rocking; ring 1: C1—N2—C6—C7—C8; ring 2: C3—C4—C5—C10—C11—C17; Ring 3: C9—C12—C13—C14—C15—C16.

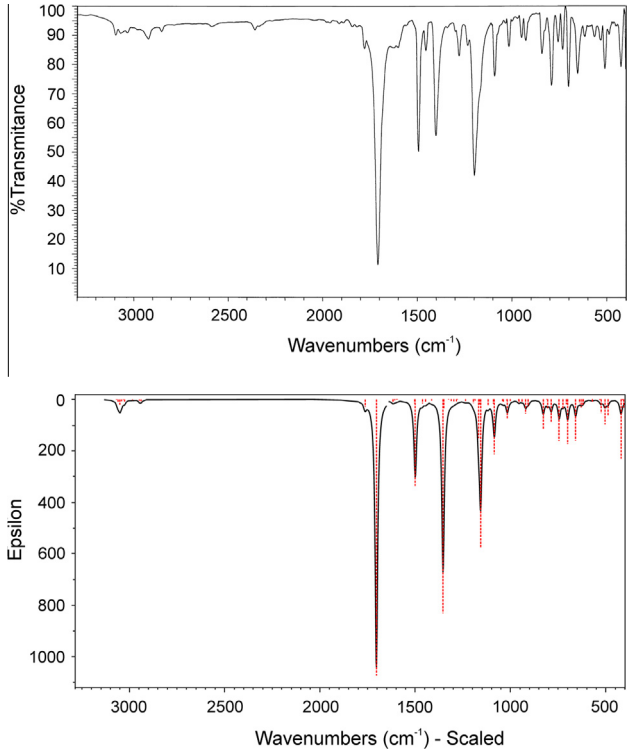

Fig. 3. Comparison of experimental (top) and theoretical (bottom) FT-IR spectra of CPPS.

bending vibrations of ring 2 of CPPS, observed at 826, 842 and 928 cm^{-1} in IR spectrum, are well supported by the computed values at 809, 827 and 938 cm^{-1}.

The in-plane C—H bending vibrations of phenyl group, ring 3, in CPPS are observed as intense bands at 1035, 1341, and 1558 cm^{-1} in FT-IR and the corresponding calculated value are 1089, 1349, and 1501 cm^{-1}. In-plane C—H bending vibration of CPPS molecule also observed at 1165 cm^{-1} in calculated spectrum and that mode is found as weak band at 1165 cm^{-1} in FT-IR. The intense IR bands at 702, 757 and 894 cm^{-1} are identified as C—H out-of-plane bending of phenyl ring and the corresponding calculated values are 698, 744 and 919 cm^{-1}. The theoretical wavenumbers of C—H in-plane and out-of-plane bending vibrations are well related to experimental ones.

The C—Cl absorption is observed in the broad region between 850 and 550 cm^{-1}, depending on the configuration and conformation of the compound [41]. When several chlorine atoms are attached to one carbon atom, the band is usually more intense and at high frequency end of the assigned interval. The bands at 424, 531, 733 and 1017 cm^{-1} in IR attributed to the C—Cl stretching vibrations (mode 73, 70, 60 and 41, Table 2). The in-plane C—Cl deformation vibrations are observed at a low frequency region of calculated IR spectrum corresponding to 257 and 277 cm^{-1}. The out-of-plane C—Cl modes are assigned to the predicted infrared wavenumbers at 169 and 344 cm^{-1}. These assignments are in good agreement with the literature [41]. The asymmetric C—Cl stretching is moderately overlapped with the C—C stretch and C—H in-plane bending modes, whereas the symmetric C—Cl stretching is mixed with the C—C stretching and C—H in-plane bending mode. C—Cl out-of-plane vibrations are effectively mixed with the out-of-plane C—H and C—C bending vibrations.

The ring C—C stretching vibrations usually occur in the region 1430–1625 cm^{-1} [42]. For aromatic six-membered rings, e.g. benzenes, there are two or three bands in this region due to skeletal vibrations, the strongest one at about 1500 cm^{-1}. In the present work, phenyl ring (ring 3) C—C stretching vibrations are observed at 1035, 1595 and 1601 cm^{-1}, in accordance with the computed values at 1089, 1597 and 1606 cm^{-1} respectively. The patterns of band observed at 1017, 1299, 1589 and 1629 cm^{-1} in FT-IR are assigned as C—C stretching vibrations of the 4-chloro-phenyl group (ring 2). The scaled theoretical wavenumbers corresponding to skeletal C—C stretching vibrations at B3LYP/6-311++G(d,p) level show excellent agreement with those observed experimentally. Beside the C—C skeletal, multiple combinations or overtones are observed in this region, related to aromatic C—H in-plane bending, CH_2 in-plane scissoring and CH_2 in-plane wagging vibrations. In the present study, the medium strong bands at 1075 and 1420 cm^{-1} in FT-IR are assigned to C—H in plane bending of the six-membered ring and CH_2 in-plane scissoring, respectively. Moreover, the skeletal C—C stretching modes are also taking a crucial part in these modes (m39 and m23) since their PED contributions are 28% and 39%, respectively. For CPPS molecule, the assignment of the skeletal C—C stretching mode in FT-IR is quite difficult, since this band is frequently masked by the more intense

bands at 1100–1400 cm^{-1} arising from the CH_2 deformation vibrations.

The region below 800 cm^{-1} is mostly dominated by in-plane and out-of-plane ring vibrations. Usually in-plane ring deformation vibrations are at higher wavenumbers than out-of-plane vibrations [43]. In the present study, the bands observed at 610, 654 and 971 cm^{-1} (m66, m63 and m46) in FT-IR are assigned to ring in-plane bending modes for ring 3, and the corresponding calculated values are 620, 657 and 1000 cm^{-1}. The in-plane C—C bending vibrations of 4-chloro-phenyl group, ring 2, in CPPS are observed as intense bands at 650 and 1000 cm^{-1} in FT-IR and the corresponding calculated values are 637 and 1015 cm^{-1}, and for ring 1, C—C bending vibration is observed at 654 cm^{-1}. The ring out-of-plane bending mode wavenumbers are observed at 488 and 510 cm^{-1}, for ring 3 and ring 2, respectively.

CH_2 group vibration

The symmetric and asymmetric stretching bands of methylene hydrogens (CH_2) were observed at 2853 and 2923 cm^{-1}. Vibrational stretching modes of methylene hydrogens correlate well with the theoretically scaled frequencies at 2937 and 2983 cm^{-1}. The theoretical description of the high-frequency range of the vibrational spectrum (CH stretching vibrations) is difficult also for other reasons than low intensity of the bands. This range may be also affected by Fermi resonance [44]. The theoretically calculated CH_2 deformation modes have been consistent with the recorded spectral data (Table 2). One of the CH_2 deformation modes called CH_2 scissoring (δCH_2) generates bands at 1420 and 1455 cm^{-1} in FT-IR. The predicted values for CH_2 scissoring modes at 1413 and 1443 cm^{-1} are matched well with that of experimental as well as the range given in the literature [45]. The medium strong band at 1234 cm^{-1} in FT-IR is attributed to CH_2 wagging (ωCH_2). The percentage of PED reveals that all the in plane CH_2 deformations are not pure modes except mode m22 for CH_2 scissoring. For methylene group of the compound, the peak at 1100 cm^{-1} in FT-IR is ascribed to methylene twisting vibrations (tCH_2). Methylene rocking vibration (ρCH_2) of the title compound display medium strong peak at 950 cm^{-1} in FT-IR.

C=O group vibrations

As far as the title compound is concerned, the region 1900–1300 cm^{-1} has very strong and sharp peaks as shown in Fig. 3. On the basis of PED, the prominent absorptions at 1708, 1780 cm^{-1} in FT-IR are assigned to C=O stretching modes. From this we found that, the intensity of these bands in FT-IR is very high. Such intense infrared absorption bands are observed due to the fact that, the multiple bonded carbonyl group is highly polar [46]. The C=O in-plane bending modes are mixed with in-plane bending modes of rings 1 and 3. The bands at 424, 610 and 791 cm^{-1} in FT-IR are assigned to C=O in-plane bending vibrations. The calculated wavenumbers at 419, 620 and 785 cm^{-1} show excellent agreement with the experimental data. The C=O out-of-plane vibrations are coupled with out-of-plane C—H vibrations and are observed at 565 and 818 cm^{-1} in FT-IR and correlate well with the computed values at 569 and 804 cm^{-1}.

C—N group vibrations

The assignment of C—N stretching modes is rather difficult task, since there are problems to discern these wavenumbers from other vibrations. Silverstein et al. [47], assigned the C—N stretching absorption in the region 1266–1382 cm^{-1} for substituted heterocyclic aromatic compounds. In the present study, C—N stretching modes are assigned on the basis of PED. The observed strong band at 1401 cm^{-1} in FT-IR is assigned to C—N stretching mode. The calculated wavenumber at 1353 cm^{-1} shows good agreement with the experimental data. It is pure mode and the PED contribution to this mode is 53%. The observed strong bands 1092 and 1198 cm^{-1} in FT-IR are also assigned to C—N stretching modes and correlate well with the computed values at 1155 and 1166 cm^{-1}. The C—N stretching modes (m38 and m35) are coupled with stretching C—C and in-plane bending C—H vibrations. The PED contributions to these modes are 17% and 13%. The C—N bending modes are coupled with in-plane bending C—C, and torsion ring vibrations for ring 3. In FT-IR, band at 894 cm^{-1} is designated as C—N in-plane bending mode. The PED contribution to this mode is about 50%. In the present work, the calculated theoretical wavenumber 657 cm^{-1} depicted in Table 2 is assigned as C—N out-of-plane vibration. The experimental counterpart in FT-IR is observed at 654 cm^{-1}.

^{13}C and ^{1}H NMR spectral analysis and solvent effects

The NMR spectroscopy is currently used for structure and functional determination of biological macromolecules. Chemical shifts contained in NMR spectra are important part of the information on molecular structure. They are valuable for structural investigations due to their sensitivity to conformational variations. A powerful way to predict and interpret the structure of large molecules is to combine computer simulation and NMR methods. Accurate predictions of molecular geometries are essential for reliable calculations of magnetic properties. Therefore, full geometry optimization of CPPS was performed by using B3LYP/6-311++G(d,p) method and GIAO ^{1}H and ^{13}C chemical shift calculations of the title compound have been made by same method. The experimental and theoretical values for ^{1}H and ^{13}C NMR of the CPPS are given in Tables 3 and 4. The NMR spectrum of CPPS was recorded in both $CDCl_3$ and DMSO-d_6 and the effect of solvent is described in detail Figs. S2–S5 (Supplementary material). In ^{1}H NMR spectra two doublets of doublets at 3.00/2.95 and 3.37/3.34 ppm in $CDCl_3$/DMSO solution mark the methylene hydrogens in the succinimide ring (Table 3). The calculated chemical shift values for methylene hydrogen atoms (with respect to TMS) are 2.83/2.99 and 3.38/3.49 ppm in $CDCl_3$/DMSO solution. The hydrogen atom of C7C—H23 group appears at higher chemical shift of 4.18/4.34 ppm ($CDCl_3$/DMSO) due to influence of phenyl ring with theoretical peaks at 3.99/4.14 ppm. In the calculated ^{1}H NMR spectrum the chemical shift values for 4-chloro-phenyl ring (ring 2) hydrogens, (with respect to TMS) are at 7.42–7.78/7.47–7.81 ppm in $CDCl_3$/DMSO solution. The calculated chemical shift values for phenyl ring hydrogen atoms (ring 3) (with respect to TMS) are 7.57–7.84/7.63–7.82 ppm in $CDCl_3$/DMSO solution. The experimental peaks of aromatic hydrogen atoms are at 7.29–7.46/7.32–7.6 ppm and correlate well with calculated chemical shifts.

Table 3
Experimental and theoretical ^{1}H NMR isotropic chemical shifts (in ppm, with respect to TMS and in $CDCl_3$/DMSO solution) of CPPS (atom positions were numbered as in Fig. 2).

	Experimental		B3LYP/6-311++G(d,p)		
Proton	$CDCl_3$	DMSO	Gas	$CDCl_3$	DMSO
H18	7.29	7.32	7.33	7.43	7.47
H21	3.08	2.95	2.67	2.83	2.99
H22	3.37	3.34	3.13	3.38	3.49
H23	4.19	4.30	3.68	3.99	4.14
H24	7.43	7.58	7.66	7.42	7.64
H25	7.39	7.42	7.52	7.78	7.80
H27	7.42	7.44	7.61	7.76	7.81
H28	7.31	7.33	7.35	7.66	7.70
H29	7.34	7.38	7.50	7.57	7.63
H30	7.36	7.40	7.52	7.63	7.67
H31	7.41	7.43	7.55	7.65	7.65
H32	7.46	7.60	7.72	7.84	7.82

Table 4
Experimental and theoretical ^{13}C NMR isotropic chemical shifts (in ppm, with respect to TMS and in $CDCl_3$/DMSO solution) of CPPS (atom positions were numbered as in Fig. 2).

Carbon	Experimental		B3LYP/6-311++G(d,p)		
	$CDCl_3$	DMSO	Gas	$CDCl_3$	DMSO
C1	176.32	177.03	182.62	188.18	190.17
C3	130.32	131.46	138.65	140.56	141.66
C4	129.37	128.98	133.84	137.26	138.52
C5	129.37	128.98	133.89	137.32	138.07
C6	174.78	175.17	181.26	185.48	187.43
C7	45.91	45.82	52.54	54.51	54.98
C8	37.12	37.13	42.37	44.68	45.25
C9	134.47	132.83	148.24	148.28	148.38
C10	129.32	128.91	134.53	136.23	137.18
C11	136.84	137.82	149.76	151.37	152.03
C12	127.33	127.42	129.98	132.68	132.89
C13	127.33	127.42	137.99	138.72	138.53
C14	128.16	128.71	136.05	136.96	137.27
C15	128.16	128.71	135.35	135.65	136.02
C16	127.63	128.22	134.34	134.88	134.66
C17	129.32	128.91	134.54	136.36	137.29

The results in Table 4 shows that the range ^{13}C NMR chemical shift of CPPS-type organic molecule is usually >100 ppm [35], the accuracy ensures reliable interpretation of spectroscopic parameters. In our present study, chemical shift of title molecule also falls with the above literature data except with the methylene and C—H groups of the succinimide ring. In the present study, signals at 37.12/37.13 ppm are assigned to methylene C8 carbon in $CDCl_3$/DMSO solution, the calculated chemical shifts for this atom by B3LYP/6-311++G(d,p) method fall at 44.68/45.25 ppm ($CDCl_3$/DMSO). The signals at 45.91/45.82 are assigned to C7 carbon in $CDCl_3$/DMSO solution, the theoretically calculated chemical shift for this atom falls at 54.51/54.98 ppm ($CDCl_3$/DMSO). The carbon atoms C7 and C8 in succinimide ring appear at lower chemical shift due to neighboring electronegative carbonyl groups. On the basis of ^{13}C NMR spectra, in which the phenyl carbon attached to the chlorine atom Cl26 has theoretical peak at 151.37 and 152.03 ppm with respect to TMS in $CDCl_3$/DMSO solution, the peaks appearing at 136.84/137.82 ppm in experimental spectra are assigned to the atom C11. In the present study, signals for aromatic carbons were observed at 129.37/128.98, 129.32/128.91 for the ring 2 and 127.33/127.42, 127.63/128.22, 128.16/128.71, 134.47/132.83 ppm for the ring 3 in ^{13}C NMR spectrum for the title molecule in $CDCl_3$/DMSO solution. The two carbon atoms (C1 and C6) of carbonyl groups resonating at 176.32/177.03 and 174.78/175.17 ppm in the ^{13}C NMR spectra show good agreement with computed values 188.18/190.17 and 185.48/187.43 ppm, in $CDCl_3$/DMSO solution.

The observed chemical shifts of investigated molecules depend on the molecular structure and on the interactions between the molecule and the surrounding solvent molecules. In nonpolar solvents, such as hydrocarbons, there are only weak interactions between solute and solvent (van der Waals or London type of interactions), and the solvent has minimal effect on the observed chemical shifts. In polar solvents such as chloroform or dimethyl sulfoxide, there are stronger dipole interactions between solvent and solute, especially if the solute molecule also contains polar bonds.

In our present work, the spectra recorded in $CDCl_3$ do not show much change compared to the experimental spectra in both ^1H NMR and ^{13}C NMR (Tables 3 and 4). In the case of DMSO-d_6, ^1H NMR (for most of the protons) and ^{13}C spectrum seems to be also unaffected. Thus, the solvent effect is very small on the chemical shifts of CPPS.

From correlation graphs, it is inferred that spectra recorded in $CDCl_3$ and DMSO-d_6 showed good correlation with the computed values, Figs. S6–S9 (Supplementary material).

Energetics and dipole moments

In order to evaluate the total energy and dipole moment behavior of two conformers **I** and **II** of CPPS in solvent media, we carried out calculations in six solvents $CHCl_3$, CH_2ClCH_2Cl, C_2H_5OH, DMF, DMSO, H_2O. The total energies and dipole moments were calculated in solvent media at the B3LYP/6-31G(d,p) level using the CPCM method and the results are given in Table 5. To find stable conformers of CPPS in different solvents, detailed conformational analyzes were carried out for the title compound. Then full geometry optimizations of these structures were performed by B3LYP/6-31G(d,p) method. The PES scans in different media are performed for CPPS using the same level of theory are shown in Fig. S10 (Supplementary material). During the calculations,all the geometrical parameters were simultaneously relaxed while the dihedral angle C1—N2—C3—C4 (around N2—C3 bond) was varied form 0° to 180° by steps of 5°. For this rotation PE curves show two energy minima at ~40° (conformer **I**) and 140° (conformer **II**), in all solvents, as shown in Fig. S10.

From Table 5, we can conclude that the obtained total energy of conformers **I** and **II** decreases with the increasing polarity of the solvent, i.e. stability of conformers increases. Also, the energy difference (ΔE) between the energies of conformers **I** and **II** in gas phase and solvent media is calculated and shown in Table 5. As can be seen from this table, in vacuum and less-polar solvents such as $CHCl_3$ and CH_2ClCH_2Cl, conformer **I** is more stable than conformer **II**, but in more polar solvents conformer **II** is a more stable one. This behavior may be result of increased repulsion of carbonyl groups of succinimide and *ortho*-hydrogen atoms of 4-chloro-phenyl group. These repulsions increase with the polarity of solvent so in more polar solvents conformer **I** is less stable.

The dipole moment is an important electronic property of a molecule. The trend in the total energies is not observed in the dipole moments. Based on predicted dipole moment values, we can say that in going from the gas phase to the solvent phase, the dipole moment value increases (Table 5). Also, the dipole moments obtained for the CPCM method increase with the increasing solvent

Table 5
Theoretical energies E (a.u.) and dipole moments η (Debye) of the conformers I and II of CPPS in different solvents, calculated at the B3LYP/6-31G(d,p) level using the CPCM method.

Media	ε	Conformer **I**		Conformer **II**		$\Delta E = E(\mathbf{I}) - E(\mathbf{II})$ (kcal/mol)
		$E(\mathbf{I})$ (a.u.)	η (Debye)	$E(\mathbf{II})$ (a.u.)	η (Debye)	
Vacuum	1.000	−1282.377945	3.847	−1282.377811	3.807	0.084
$CHCl_3$	4.711	−1282.388334	4.356	−1282.388310	4.316	0.015
CH_2ClCH_2Cl	10.125	−1282.390082	4.444	−1282.390078	4.402	0.002
C_2H_5OH	24.852	−1282.391012	4.490	−1282.391023	4.444	−0.007
DMF	37.219	−1282.391228	4.501	−1282.391242	4.456	−0.009
DMSO	46.826	−1282.391317	4.506	−1282.391332	4.460	−0.010
H_2O	78.355	−1282.391457	4.513	−1282.391475	4.463	−0.011

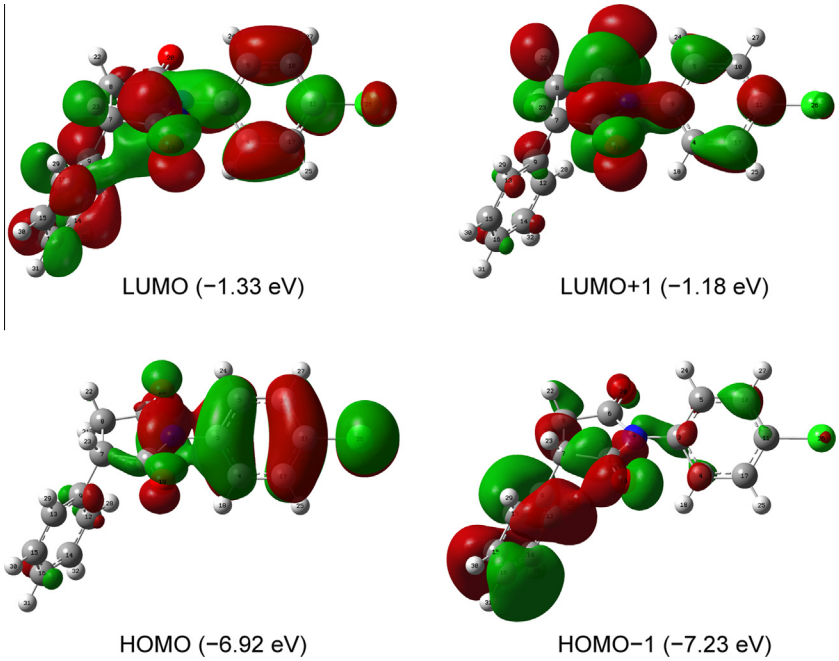

Fig. 4. Molecular orbital surfaces and energies for the HOMO − 1, HOMO, LUMO and LUMO + 1 orbitals of CPCM.

polarity. Solvent stabilize charge separation in the molecules, therefore, enhancing the rise of dipole moments.

Frontier molecular orbitals

The frontier orbitals, HOMO and LUMO determine the way how the molecule interacts with other species and helps to characterize the chemical reactivity and kinetic stability of the molecule [48]. They play an important role in the electric and optical properties, as well as in the UV–Vis spectra and chemical reactions. HOMO energy determines the ability to donate an electron and LUMO energy determines the ability to accept an electron. The energy gap between the HOMO and LUMO is very important in determining the chemical (re)activity of the molecule. A small HOMO–LUMO energy gap implies low kinetic stability, because it is energetically favorable to add electrons to a low-lying LUMO and to receive electrons from a high-lying HOMO [49]. Thus, molecules with low frontier orbital gap are more polarizable and associated with high chemical reactivity. Fig. 4 shows the distributions HOMO−1, HOMO, LUMO and LUMO+1 orbital's computed at the B3LYP/6-311++G(d,p) level for the CPPS. The calculations indicate that the title compound has (74) occupied molecular orbitals. Recently the energy gap between HOMO and the LUMO has been used to prove the bioactivity from intramolecular charge transfer (ICT). Both the HOMOs and the LUMOs are mainly localized on the rings indicating that the HOMO and LUMO are mostly the π-type orbitals. As seen from Fig. 4, in the HOMO−1, and HOMO, electrons are mainly delocalized on the phenyl and 4-chloro-phenyl group. On the other hand, the lowest unoccupied molecular orbitals are localized mainly on succinimide ring as shown in Fig. 4. The HOMO lying at −6.92 eV (computed by TD-DFT), and the LUMO lying at −1.33 eV HOMO (orbital 74) → LUMO (orbital 75) transition implies an ED transfer to succinimide group from the phenyl rings ($\pi \rightarrow \pi^*$ transition) and from the lone pair on chlorine atom. The energy difference between the HOMO and LUMO was obtained as 5.58 eV in the gas phase calculations. With this large energy gap, it can be said that the title molecule has high kinetic stability and low chemical reactivity.

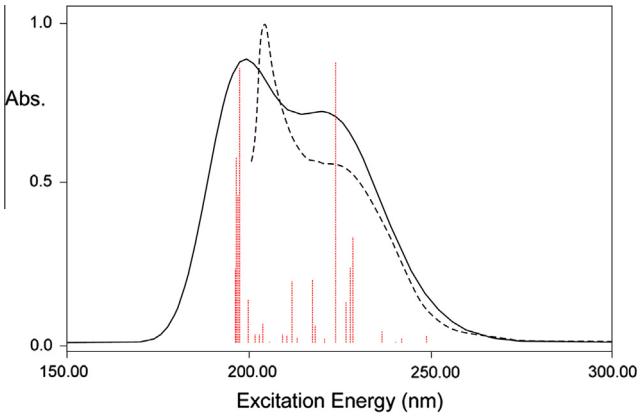

Fig. 5. Experimental (dashed line) and simulated (full line) UV absorption spectra of CPPS in ethanol.

UV–Vis studies and electronic properties

On the basis of a fully optimized ground-state structure, TD-DFT has been used to determine the low-lying excited states of CPPS. The electronic spectra of CPPS were computed in the gas phase and the ethanol environments. The solvent effect was calculated using CPCM method. The electronic absorption spectrum of the title compound in ethanol was recorded within the 200–500 nm range and the representative spectrum of computed transitions plot on the experimental is shown in Fig. 5. The computed result shows that the HOMO to LUMO transition corresponds to the λ max absorption band in the UV–Vis spectrum. The calculated results involving the vertical excitation energies (E), oscillator strength (f) and wavelength (λ) are compared with measured experimental wavelengths (Table 6). As can be seen from Fig. 5, electronic absorption spectrum of CPPS shows two bands at 202 and 224 nm. From TD-DFT calculation, the most significant theoretical absorption bands are predicted at 197, 223 and 228 nm and can easily be seen that they correspond well with the

Table 6
Experimental and calculated absorption wavelength λ (nm), excitation energies E (eV), oscillator strengths (f) of the most significant singlet excited states for CPPS at the B3LYP/6-311++G(d,p) level of theory.

Transition	Experimental λ (nm)	TD-DFT method /Ethanol			TD-DFT method/Gas phase		
		λ (nm)	Excitation energy E (eV)	Oscillator strength f	λ (nm)	Excitation energy E (eV)	Oscillator strength f
I	224	228	5.44 (74 → 75)	0.066	244	5.07 (74 → 75)	0.138
II		227	5.45 (73 → 75)	0.047	240	5.17 (74 → 76)	0.236
II		223	5.55 (73 → 76)	0.176	237	5.23 (72 → 75)	0.019
IV	202	197	6.30 (71 → 76)	0.172	227	5.46 (73 → 75)	0.011
V		196	6.33 (70 → 78)	0.116	195	6.37 (69 → 75)	0.179

Table 7
Second order perturbation theory analysis of Fock matrix in NBO basis.

Donor (i)	Type	ED (i) (e)	Acceptor (j)	Type	ED (j) (e)	$E(2)$ (kcal/mol)	$E(j) - E(i)$ (a.u.)	$F(i,j)$ (a.u.)
C1—N2	σ	1.9827	N2—C3	σ*	0.04202	1.83	1.18	0.042
C1—N2	σ		N2—C6	σ*	0.10123	0.86	1.19	0.029
C1—N2	σ		C6—O20	σ*	0.0113	2.97	1.42	0.058
C1—O19	σ		C1—C7	σ*	0.0781	1.52	1.46	0.043
C1—O19	π	1.988	C1—O19	π*	0.21664	0.54	0.4	0.014
C1—O19	π		C7—C9	σ*	0.02746	0.75	0.8	0.022
N2—C3	σ	1.9836	C1—N2	σ*	0.10062	1.46	1.18	0.038
N2—C3	σ		N2—C6	σ*	0.10123	1.39	1.18	0.037
N2—C3	σ		C3—C4	σ*	0.02372	1.1	1.36	0.035
N2—C3	σ		C3—C5	σ*	0.0238	1.12	1.36	0.035
N2—C6	σ	1.9831	C1—N2	σ*	0.10062	0.88	1.19	0.03
N2—C6	σ		C1—O19	σ*	0.01137	3.04	1.42	0.059
N2—C6	σ		N2—C3	σ*	0.04202	1.81	1.18	0.041
C3—C4	σ	1.9724	C3—C5	σ*	0.0238	4.47	1.28	0.067
C3—C4	σ		C4—C17	σ*	0.01483	2.83	1.29	0.054
C3—C5	π	1.6585	C4—C17	π*	0.31626	20.99	0.29	0.07
C3—C5	π		C10—C11	π*	0.3905	20.34	0.28	0.068
C4—C17	σ	1.9683	N2—C3	σ*	0.04202	4.18	1.08	0.06
C4—C17	σ		C3—C4	σ*	0.02372	3.09	1.27	0.056
C4—C17	π	1.6617	C3—C5	π*	0.3697	19.91	0.28	0.067
C4—C17	π		C10—C11	π*	0.3905	21.34	0.27	0.069
C5—C10	σ	1.9683	N2—C3	σ*	0.04202	4.24	1.08	0.061
C5—C10	σ		C3—C5	σ*	0.0238	3.09	1.27	0.056
C5—C10	σ		C10—C11	σ*	0.02778	3.6	1.27	0.06
C5—C10	σ		C11—Cl26	σ*	0.03265	5.05	0.85	0.059
C6—O20	σ	1.9944	C6—C8	σ*	0.0627	1.45	1.47	0.042
C6—O20	π	1.9891	C6—O20	π*	0.22275	0.58	0.4	0.014
C7—C8	σ	1.9706	C1—O19	σ*	0.01137	3.93	1.23	0.062
C7—C8	σ		C6—O20	σ*	0.0113	4.09	1.23	0.064
C7—H23	σ	1.9622	C1—O19	π*	0.21664	4.27	0.52	0.044
C7—H23	σ		C9—C12	σ*	0.02566	4.37	1.08	0.062
C8—H21	σ	1.9699	C6—O20	π*	0.22275	3.89	0.53	0.043
C8—H22	σ	1.9647	C6—O20	π*	0.22275	5.2	0.53	0.049
C9—C13	π	1.6589	C12—C14	π*	0.32641	19.95	0.28	0.067
C9—C13	π		C15—C16	π*	0.32361	20.35	0.28	0.068
C10—C11	π	1.6737	C3—C5	π*	0.3697	19.6	0.29	0.069
C10—C11	π		C4—C17	π*	0.31626	19.08	0.3	0.067
C12—C14	π	1.6715	C9—C13	π*	0.3475	21.09	0.29	0.07
C12—C14	π		C15—C16	π*	0.32361	19.55	0.29	0.067
C15—C16	π	1.6601	C9—C13	π*	0.3475	20.31	0.28	0.068
C15—C16	π		C12—C14	π*	0.32641	20.87	0.28	0.068
N2	LP(1)	1.6041	C1—O19	π*	0.21664	46.25	0.29	0.108
N2	LP(1)		C3—C5	π*	0.3697	12.48	0.3	0.055
N2	LP(1)		C6—O20	π*	0.22275	46.32	0.28	0.107
O19	LP(2)	1.8435	C1—N2	σ*	0.10062	30.4	0.65	0.128
O19	LP(2)		C1—C7	σ*	0.0781	21.14	0.62	0.104
O20	LP(2)	1.8481	N2—C6	σ*	0.10123	30.18	0.65	0.127
O20	LP(2)		C6—C8	σ*	0.0627	20.03	0.64	0.103
Cl26	LP(1)	1.992	C10—C11	σ*	0.02778	1.63	1.49	0.044
Cl26	LP(1)		C11—C17	σ*	0.02779	1.63	1.49	0.044
Cl26	LP(2)	1.9717	C10—C11	σ*	0.02778	4.15	0.88	0.054
Cl26	LP(2)		C11—C17	σ*	0.02779	4.15	0.88	0.054
Cl26	LP(3)	1.9276	C10—C11	π*	0.3905	12.5	0.33	0.062
C10—C11	π*	0.3905	C3—C5	π*	0.3697	327.57	0.01	0.085
C10—C11	π*		C4—C17	π*	0.31626	204.66	0.01	0.08

experimental. The TD-DFT calculation predicts one electronic transition at 228 nm with an oscillator strength $f = 0.0663$, in good agreement with the experimentally measured narrow shoulder at 224 nm in ethanol as shown in Fig. 5. This electronic absorption corresponds to the transition from the ground to the first excited state and is mainly described by one electron excitation from the

HOMO to the LUMO. The first dipole allows (74 → 75) in the gas phase at 244 nm with higher oscillation strength of 0.1376. The next transition is at HOMO−1, (orbital 73) → LUMO (orbital 75) and HOMO (orbital 74)→LUMO+1 (orbital 76), in ethanol and gas, with oscillation strength of 0.047 and 0.2358, respectively. From Fig. 5, it is evident that the one intense band at 204 nm in experimental UV spectrum in ethanol is concerned with the HOMO−3, (orbital 71) → LUMO (orbital 75) electronic transitions, and the corresponding theoretical peak is found in the TD-DFT UV spectra in ethanol/gas phase is at 197 nm and 227 nm.

NBO analysis

NBO analysis has been performed on CPPS molecule using NBO 3.1 program as implemented in the Gaussian 03 package at the B3LYP/6-311++G(d,p) level in order to elucidate ICT and delocalization of ED within the molecule. A useful feature of the NBO method is that it gives information about interactions in filled and virtual orbital spaces that could improve the analysis of intra- and intermolecular interactions. It also provides a convenient basis for investigating charge transfer or conjugative interaction in molecular systems. The larger the $E(2)$ value (energy of hyperconjugative interactions), the more intensive is the interaction between electron donors and electron acceptors. Furthermore, the more donating tendency from electron donors to electron acceptors is the main requirement for the greater conjugation in the investigated system. Delocalization of ED between occupied Lewis-type (bonding or lone pair) NBO's and formally unoccupied (antibonding or Rydberg) non-Lewis NBO's correspond to a stabilizing donor–acceptor interaction. The important interactions between 'filled' (donor) Lewis type NBO's and 'empty' (acceptor) non Lewis NBO's of title molecule are given in Table 7.

In CPPS the intramolecular interactions are formed by the orbital overlap between bonding C—C, C—N, C—H and C=O antibonding orbitals which results in ICT causing stabilization of the molecule. These interactions are observed due to an increase in ED in C—C, C—N, C—H and C=O antibonding orbitals that weakens the respective bonds. The strong intramolecular hyperconjugative interaction of the σ and π electrons of C—C to the anti C—C bond of the succinimide ring (ring 1) leads to stabilization of some part of the ring 1 as evident from Table 7. For example: the intramolecular hyperconjugative interaction of σ(C1—N2) distributes to σ*(N2—C3), N2—C6, C6—O20, leading to stabilization of 0.86–3 kcal/mol. The same kind of interaction is calculated in the N2—C3, N2—C6, C7—C8, C7—H23 bond, as shown in Table 7. The interaction energy, related to the resonance in the molecule, is electron withdrawing to the ring through σ*(C1—N2, C1—C7 and N2—C6, C6—C8) bond from the lone pairs LP(2)O19 and LP(2)O20 which leads to moderate stabilization energy of 20–30 kcal/mol as shown in Table 7. The most important interaction energies of LP(1)N2 → π*(C1—O19) and LP(1)N2 → π*(C1—O20) are 46.25 and 46.32 kcal/mol respectively. The magnitude of charge transfer from the lone pairs of Cl26 to anti-bonding C10—C11 and C11—C17, σ orbitals amount to stabilization of 4 kcal/mol, while the ICT to anti-bonding π orbital (C10—C11), brings stabilization of the order of 12.5 kcal/mol.

The second order perturbation theory analysis of Fock matrix in NBO basis of CPPS (Table 7) also indicates intramolecular interactions due to the orbital overlap of π(C—C) and π*(C—C) in phenyl rings 2 and 3, resulting in high ED (approx. 0.3162–0.3905 e) of anti-bonding π orbitals (C—C). The orbital overlap in phenyl rings 2 and 3 between π(C—C) and π*(C—C) results in ICT causing stabilization of the whole system. The delocalization of electron π*(C10—C11) to π*(C3—C5) and to π*(C4—C17) goes with enormous stabilization energy of 327.57 and 204.66 kcal/mol.

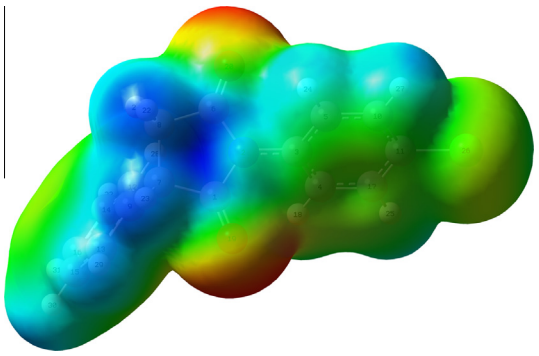

Fig. 6. Electrostatic potentials of CPPS (B3LYP/6-311++G(d,p), 0.002 a.u., energy values −35.89 to +35.89 kcal/mol); color coding: red (very negative), orange (negative), yellow (slightly negative), green (neutral), turquoise (slightly positive), light blue (positive), dark blue (very positive). (For interpretation of the references to color in this figure legend, the reader may have a look at the web version of the article.)

Molecular electrostatic potential

The MEP at a point in space around a molecule gives information about the net electrostatic effect produced at that point by total charge distribution of the molecule. Moreover, MEP surface helps to predict the reactivity of wide variety of biomolecules in electrophilic and nucleophilic reactions, the study of biological recognition processes and hydrogen bonding interactions. It also provides visual understanding of relative polarity of the molecule. An electron density isosurface mapped with electrostatic potential surface depicts the size, shape, charge density and reactive sites of the molecules. The different values of the electrostatic potential at the surface are represented by different colors; red represents regions of most negative electrostatic potential, blue represents regions of most positive electrostatic potential and green represents regions close to zero potential. The electrostatic potential increases in the order red < orange < yellow < green < blue [50]. To predict reactive sites for electrophilic and nucleophilic attack, MEP surface is plotted over optimized geometry of stable isomer **I** of CPPS at B3LYP/6-311++G(d,p) level. As can be easily seen in Fig. 6, investigated molecule has several possible sites for electrophilic and nucleophilic attack. The electrostatic potential ranges from −35.89 to +35.89 kcal/mol with dark blue denoting extremely electron-deficient regions ($V(r) > 35.89$ kcal/mol) and red denoting electron rich regions ($V(r) < -35.89$ kcal/mol). As can be seen from the figure, negative region is mainly localized over the oxygen atoms (O19 and O20) of the carbonyl groups. The maximum positive region is localized on the C7—H and C8—H bonds of succinimide ring indicating a possible site for nucleophilic attack. These sites give information about the region from where the compound can have intermolecular interactions. Molecular electrostatic potential surface map indicates that the most suitable atomic sites for electrophilic attack are O19 and O20 atoms, while the most probable sites which could be involved in nucleophilic process are at C7—H and C8—H bonds of succinimide ring. It is interesting to note that the chlorine atom presents the less-negative potential having the reddish-yellow color in the MEP surface.

Conclusions

Based on the density functional theory B3LYP/6-311++G(d,p) method, structural, vibrational, NMR, electronic and reactivity aspects of 1-(4-chloro-phenyl)-3-phenyl-succinimide were studied in detail and the results were also compared with the experiment.

A complete vibrational dynamical and molecular structure analysis of CPPS has been done, based on the quantum chemical approach by DFT calculations. The spectral characterization studies, such as FT-IR and NMR for CPPS, have been carried out for the first time. A good agreement between experimental and calculated vibrations normal modes has been found. The NBO result reflects the charge transfer from phenyl rings 2 and 3, to the succinimide ring, due to the orbital overlap of π(C—C) and π^*(C—C). The experimental and theoretical UV–Vis spectral analysis has also provided insight into the excitation energy and oscillator strength and predicted mainly the $\pi \rightarrow \pi^*$ type electronic transitions which are intra-molecular charge transfer type. It is seen that the enthalpies decrease and dipole moments increase with the increasing the polarity of solvent. The MEP map shows the negative potential sites are on oxygen atoms as well as the positive potential sites are around the hydrogen atoms of C—H in succinimide ring. The present quantum chemical study may lead to the understanding of properties and activity of CPPS and may also help in its use for more advance applications. We hope our results will be of assistance in the quest of the experimental and theoretical evidence for the title molecule in molecular bindings and will also be helpful for the design and synthesis of new drugs.

Acknowledgments

This work has been financially supported by Ministry of Education and Science, Republic of Serbia, under Grant Nos. 172035, 172013 and High-Performance Computing Infrastructure for South East Europe's Research Communities (HP-SEE Contract Number 261499, http://www.hp-see.eu/).

Appendix A. Supplementary material

Supplementary data associated with this article can be found, in the online version, at http://dx.doi.org/10.1016/j.saa.2013.07.099.

References

[1] P.N. Patsalos, Epilepsia 46 (2005) 140–144.
[2] J.C. Rekling, Neurosci. Lett. 335 (2003) 167–170.
[3] K. Evason, C. Huang, I. Yamben, D.F. Covey, K. Kornfeld, Science 307 (2005) 258–262.
[4] E. Pourcher, B. Gomez-Mancilla, P.J. Bédard, Mov. Disord. 7 (1992) 132–136.
[5] J.H. Jadhav, J.J. Balsara, A.J. Jeurkar, A.G. Chandorkar, Indian J. Physiol. Pharmacol. 25 (1981) 274–278.
[6] H. Kaneto, S. Kawatani, H. Kaneda, Jpn. J. Psychopharmacol. 6 (1986) 267–273.
[7] R.J. Porter, J.K. Penry, J.R. Lacy, M.E. Newmark, H.J. Kupferberg, Neurology 29 (1979) 1509–1513.
[8] G. Cheng, J.K. Weston, A.C. Jr, Bratton, Epilepsia 4 (1963) 66–76.
[9] P. Moreau, F. Anizon, M. Sancelme, M. Prudhomme, C. Bailly, D. Sevère, J.-F. Riou, D. Fabbro, T. Meyer, A.-M. Aubertin, J. Med. Chem. 42 (1999) 584–592.
[10] J.A. Bush, B.H. Long, J.J. Catino, W.T. Bradner, K. Tomita, J. Antibiot. 40 (1987) 668–678.
[11] W.J. Trigg, G. Grangier, T. Lewis, M.G. Rowan, B.V.L. Potter, I.S. Blagbrough, Tetrahedron Lett. 39 (1998) 893–896.
[12] P. Dobelis, J.E. Madl, J.A. Pfister, G.D. Manners, J.P. Walrond, J. Pharmacol. Exp. Ther. 291 (1999) 538–546.
[13] K.R. Jennings, D.G. Brown, D.P. Jr., Wright, Experientia 42 (1986) 611–613.
[14] P.B. Jensen, B. Sokilde, E.V. Carstensen, S.W. Langer, A. Creighton, M. Sehested, L.H. Jensen, EP 1373494, 2004.
[15] H.F. Proelss, H.J. Lohmann, Clin. Chem. 17 (1971) 222–228.
[16] I. Magyar, R. Walsa, Therapia Hungarica 14 (1966) 97–107.
[17] B.M. Khadilkar, S.R. Bhayade, Indian J. Chem. B 32B (1993) 338–342.
[18] H.J. Schneider, G. Unger, D. Rössler, C. Bothor, W. Berg, G. Ernst, Z Urol. Nephrol. 72 (1979) 237–247.
[19] A.A. Korhalkar, B.G. Khadse, S.R. Sengupta, Indian Drugs 29 (1992) 306–307.
[20] H. Koch, J. Kotlan, Patentschrift (Switz.), 1983, CH 634482 A5 19830215.
[21] L.D. Goodhue, J.E. Mahan (to Phillips Petroleum Co.), US Patent, 2,735,225, 1956.
[22] Kunihiro Yabutani, Kasushi Takehana, Fujio Araki, Tatsuo Harada, Jpn. Kokai Tokkyo Koho (1975) JP 50129743 A 19751014.
[23] A. Fujinami, T. Ozaki, K. Nodera, K. Tanaka, Agric. Biol. Chem. 36 (1972) 318–323.
[24] N.P. Shetgiri, B.K. Nayak, Indian J. Chem. B 44B (2005) 1933–1936.
[25] K. Singhal, R. Rastogi, P. Raj, Indian J. Chem. A 26A (1987) 146–150.
[26] M.K. Hargreaves, J.G. Pritchard, H.R. Dave, Chem. Rev. 70 (1970) 439–469.
[27] N. Perišić-Janjić, R. Kaliszan, P. Wiczling, N. Milošević, G. Uščumlić, N. Banjac, Mol. Pharmaceut. 8 (2011) 555–563.
[28] M. Struga, B. Miroslaw, M. Pakosinska-Parys, A. Drzewiecka, P. Borowski, J. Kossakowski, A.E. Koziol, J. Mol. Struct. 965 (2010) 23–30.
[29] S.P.V. Chamundeeswaria, E.J. Jebaseelan Samuela, N. Sundaraganesan, Spectrochim. Acta A 83 (2011) 478–489.
[30] M.J. Frisch, G.W. Trucks, H.B. Schlegel, G.E. Scuseria, M.A. Robb, J.R. Cheeseman, J.A. Montgomery Jr., T. Vreven, K.N. Kudin, J.C. Burant, J.M. Millam, S.S. Iyengar, J. Tomasi, V. Barone, B. Mennucci, M. Cossi, G. Scalmani, N. Rega, G.A. Petersson, H. Nakatsuji, M. Hada, M. Ehara, K. Toyota, R. Fukuda, J. Hasegawa, M. Ishida, T. Nakajima, Y. Honda, O. Kitao, H. Nakai, M. Klene, X. Li, J.E. Knox, H.P. Hratchian, J.B. Cross, V. Bakken, C. Adamo, J. Jaramillo, R. Gomperts, R.E. Stratmann, O. Yazyev, A.J. Austin, R. Cammi, C. Pomelli, J.W. Ochterski, P.Y. Ayala, K. Morokuma, G.A. Voth, P. Salvador, J.J. Dannenberg, V.G. Zakrzewski, S. Dapprich, A.D. Daniels, M.C. Strain, O. Farkas, D.K. Malick, A.D. Rabuck, K. Raghavachari, J.B. Foresman, J.V. Ortiz, Q. Cui, A.G. Baboul, S. Clifford, J. Cioslowski, B.B. Stefanov, G. Liu, A. Liashenko, P. Piskorz, I. Komaromi, R.L. Martin, D.J. Fox, T. Keith, M.A. Al-Laham, C.Y. Peng, A. Nanayakkara, M. Challacombe, P.M.W. Gill, B. Johnson, W. Chen, M.W. Wong, C. Gonzalez, J.A. Pople, Gaussian 03, Revision C. 02, Gaussian, Inc., Wallingford CT, 2004.
[31] M.H. Jamróz, Vibrational Energy Distribution Analysis VEDA 4, Warsaw, 2004.
[32] W.J. Hehre, L. Radom, P.v.R. Schleyer, J.A. Pople, Ab initio Molecular Orbital Theory, Wiley, New York, 1986.
[33] C. Herrmann, M. Reiher, Top. Curr. Chem. 268 (2007) 85–132.
[34] N. Sundaraganesan, S. Ilakiamani, H. Saleem, P.M. Wojciechowski, D. Michalska, Spectrochim. Acta A 61 (2005) 2995–3001.
[35] R. Ditchfield, J. Chem. Phys. 56 (1972) 5688–5691.
[36] K. Wolinski, J.F. Hinton, P. Pulay, J. Am. Chem. Soc. 112 (1990) 8251–8260.
[37] V. Barone, M.J. Cossi, Phys. Chem. A 102 (1998) 1995–2001.
[38] E.D. Glendening, A.E. Reed, J.E. Carpenter, F. Weinhold, NBO version 3.1, TCI, University of Wisconsin, Madison, 1998.
[39] L. Vrielynck, J.P. Cornard, J.C. Merlin, M.F. Lautie, Spectrochim. Acta A 50 (1994) 2177–2188.
[40] N.B. Colthup, L.H. Daly, S.E. Wiberley, Introduction to Infrared and Raman Spectroscopy, third ed., Academic Press, Boston, 1990 (Chapter 13).
[41] J.R. Durig, M.M. Bergana, H.V. Phan, J. Raman Spectrosc. 22 (1991) 141–154.
[42] A. Teimouri, A.N. Chermahini, K. Taban, H.A. Dabbagh, Spectrochim. Acta A 72 (2009) 369–377.
[43] G. Socrates, Infrared and Raman Characteristic Group Frequencies, third ed., John Wiley & Sons, Ltd., Chichester, 2001.
[44] G. Rauhut, P. Pulay, J. Phys. Chem. 99 (1995) 3093–3100.
[45] V. Krishnakumar, V. Balachandran, T. Chithambarathanu, Spectrochim. Acta A 62 (2005) 918–925.
[46] V. Krishnakumar, G. Keresztury, T. Sundius, S. Seshadri, Spectrochim. Acta A 68 (2007) 845–850.
[47] M. Silverstein, G. Clayton Basseler, C. Morill, Spectrometric Identification of Organic Compounds, Wiley, New York, 1981.
[48] I. Fleming, Frontier Orbitals and Organic Chemical Reactions, John Wiley and Sons, New York, 1976. pp. 5–27.
[49] M.D. Diener, J.M. Alford, Nature 393 (1998) 668–671.
[50] P. Thul, V.P. Gupta, V.J. Ram, P. Tandon, Spectrochim. Acta A 75 (2010) 251–260.